

PAPER • OPEN ACCESS

Error field detection and correction studies towards ITER operation













To cite this article: L. Piron *et al* 2024 *Nucl. Fusion* **64** 066029

View the [article online](#) for updates and enhancements.

You may also like

- [Benchmarking 2D against 3D FDTD codes for the assessment of the measurement performance of a low field side plasma position reflectometer applicable to IDTT](#)
F. da Silva, E. Ricardo, J. Ferreira et al.
- [Techniques to widen the operational space of SPIDER Radio Frequency driven plasma source](#)
R Casagrande, M Dan and A Maistrello
- [On the perturbation of the interferometric phase in interferometry-polarimetry of fusion plasmas](#)
Leonardo Giudicotti, Enrico Zilli and Donatella Fiorucci

Error field detection and correction studies towards ITER operation

L. Piron^{1,2,*} , C. Paz-Soldan³ , L. Pigatto² , P. Zanca² , O. Sauter⁴ , T. Putterich⁵ , P. Bettini^{2,6} , M. Bonotto² , G. Cunningham⁷, G. De Tommasi⁸ , N. Ferron², M. Gambrioli^{2,9}, G. Graham⁷, P. De Vries¹⁰ , Y. Gribov¹⁰, Q. Hu¹¹ , K. Kirov⁷, N.C. Logan³ , M. Lennholm⁷ , M. Mattei⁸ , M. Maraschek⁵, T. Markovic¹², G. Manduchi^{2,13}, P. Martin^{1,2}, A. Pironti⁸, A.R. Polevoi¹⁰, T. Ravensbergen¹⁰ , D. Ryan⁷ , B. Sieglin⁵ , W. Suttrop⁵ , D. Terranova^{2,13} , W. Teschke⁵, D.F. Valcarcel⁷, C. Vincent⁷, JET Contributors^a, the EUROfusion Tokamak Exploitation Team^b, the ASDEX Upgrade Team^c and MAST-U Team^d

¹ Department of Physics and Astronomy, University of Padova, Padova, Italy

² Consorzio RFX (CNR, ENEA, INFN, Università di Padova, Acciaierie Venete SpA), C.so Stati Uniti 4, 35127 Padova, Italy

³ Department of Applied Physics & Applied Mathematics, Columbia University, New York, NY 10027, United States of America

⁴ École Polytechnique Fédérale de Lausanne (EPFL), Swiss Plasma Center (SPC), CH-1015 Lausanne, Switzerland

⁵ Max-Planck-Institut für Plasma Physik, Garching, Germany

⁶ Department of Electrical Engineering, University of Padova, Padova, Italy

⁷ Culham Science Centre, Abingdon, United Kingdom of Great Britain and Northern Ireland

⁸ Università Federico II, Napoli, Italy

⁹ CRF—University of Padova, Padova, Italy

¹⁰ ITER Organization, Cadarache, France

¹¹ Princeton Plasma Physics Laboratory, Princeton, NJ 08540, United States of America

¹² Institute of Plasma Physics of the CAS, Prague, Czech Republic

¹³ Istituto per la Scienza e la Tecnologia dei Plasmi, CNR, Padova, Italy

E-mail: lidia.piron@igi.cnr.it

Received 16 January 2024, revised 26 March 2024

Accepted for publication 17 April 2024

Published 9 May 2024



CrossMark

Abstract

In magnetic fusion devices, error field (EF) sources, spurious magnetic field perturbations, need to be identified and corrected for safe and stable (disruption-free) tokamak operation. Within Work Package Tokamak Exploitation RT04, a series of studies have been carried out to test the portability of the novel non-disruptive method, designed and tested in DIII-D (Paz-Soldan *et al* 2022 *Nucl. Fusion* **62** 126007), and to perform an assessment of model-based EF control strategies towards their applicability in ITER. In this paper, the lessons learned, the physical mechanism behind the magnetic island healing, which relies on enhanced viscous torque that

^a See Maggi *et al* 2024 (<https://doi.org/10.1088/1741-4326/ad3e16>) for JET Contributors.

^b See Joffrin *et al* 2024 (<https://doi.org/10.1088/1741-4326/ad2be4>) for the EUROfusion Tokamak Exploitation Team.

^c See Zohm *et al* 2024 (<https://doi.org/10.1088/1741-4326/ad249d>) for the ASDEX Upgrade Team.

^d See the author list of 'MAST Upgrade Results Towards Integrating High Core Confinement and Divertor Power Dissipation' by J Harrison *et al* to be published in *Nuclear Fusion Special Issue: Overview and Summary Papers from the 29th Fusion Energy Conference (London, UK, 16–21 October 2023)*.

* Author to whom any correspondence should be addressed.



Original content from this work may be used under the terms of the [Creative Commons Attribution 4.0 licence](https://creativecommons.org/licenses/by/4.0/). Any further distribution of this work must maintain attribution to the author(s) and the title of the work, journal citation and DOI.

acts against the static electro-magnetic torque, and the main control achievements are reported, together with the first design of the asynchronous EF correction current/density controller for ITER.

Keywords: error fields, plasma control, ITER

(Some figures may appear in colour only in the online journal)

1. Introduction

Error fields (EFs) are the long wavelength component of any non-axisymmetric fields present in tokamaks, which are due to unavoidable imperfections associated with misalignments and deviations occurred in the manufacture and assembly of the magnets, current feeds, eddy currents associated with 3D wall structures, magnetized ferromagnetic components of the machine and in the vicinity of the plasma, etc [1]. EFs can interact with the tokamak plasma through multiple mechanisms, such as rotation braking, confinement degradation, energetic particles losses, MHD triggering, potentially driving a plasma disruption [2].

For EF detection and control, ITER is equipped with 18 superconducting correction coils, named here EFCC, located external to the vacuum vessel, 6 in the upper, midplane and lower rows, as reported in red in figure 1. The EFCCs will be connected to 9 independent power supplies and will be used for the identification and the minimization of $n = 1$ EFs. In addition to this EFCC set, 27 ELM control coils, located internal to the vacuum vessel, will be available, 9 in the upper, midplane and lower rows, as shown in blue in figure 1. The ELM coils will be connected to 27 independent power supplies and will be used for the identification and correction of $n = 1$ and $n = 2$ EFs in scenarios when these coils are not used for ELM control or in scenarios when the coil currents required for the ELM control leave sufficient margin.

At the beginning of ITER commissioning, such EF actuators will be exploited to identify EFs. For this purpose, the compass scan method has been standardly executed [3] in various magnetic fusion devices, such as NSTX [4], ALCATOR-CMOD [5], ASDEX-Upgrade [6], JET [7, 8], MAST [9, 10], EAST [11], DIII-D [12, 13], KSTAR [14] and RFX-mod [15]. This method is based on the assumption that the magnetic island formation (locked mode) for a given ohmic plasma scenario, during the magnetic field penetration process, depends only on the amplitude of the total non-axisymmetric field, B_{tot} . The total non-axisymmetric field is the sum of the externally applied magnetic field, the non-axisymmetric component of the externally applied magnetic field, and the EF one. The critical threshold value of the external field should lie on a circle in the complex ($\text{Re}(B_{\text{tot}})$, ($\text{Im} B_{\text{tot}}$)) plane. The EF topology, i.e. amplitude and phase, is inferred from the possible shift of this circle that is obtained by measuring the locked mode onset, as the external magnetic field is ramped with several different toroidal phases.

However, the compass scan is challenged by the requirement of exciting magnetic island with a potential disruptive nature. Such kind of dynamics cannot be tolerated in future

disruption-averse tokamaks such as ITER [16] and SPARC. This issue has been solved in the novel non-disruptive compass scan method [17], which has been designed and tested in DIII-D and relies on magnetic island healing. Recently, such a novel method has been executed in JET and in MAST-U, as documented in this paper, to assess its portability among magnetic fusion devices.

Once the EF source has been identified, the correction currents for its minimization are yielded, which can be used in a pre-programmed way during plasma operations. Note that such empirically identified EF correction strategy represents the optimum point of correction in a given coil configuration.

Besides empirical EF correction, control strategies based on an accurate description of the EF sources by electromagnetic modelling coupled with the plasma response by the IPEC code have been shown to be a promising route for minimizing the EF components that couple strongly to the plasma resulting in increased drive for magnetic islands [18, 19]. A comparison of IPEC predictions against empirical $n = 1$ EF control currents in DIII-D, in both ohmic and H-mode plasmas, found good agreement [20].

In this context, model-based EF correction strategies have been recently tested in ASDEX-Upgrade, which improved achievable β_N by 10% [21] and allowed the exploration of the lowest density in the low torque regime. The main insights of this plasma response EF modelling, documented here, help to establish the basis for designing current feedback control for the coils able to track the pre-programmed correction currents for a given coil configuration and target equilibrium.

In this paper, the portability of the non-disruptive compass scan method for EF identification in DIII-D, JET, and MAST-U devices is presented in section 2, along with the lessons learned. The modelling of the physical mechanism behind magnetic island healing is provided in section 3. The development of functionalities for EF identification studies in ITER is described in section 4 and the main results achieved on model-based EF control in AUG are reported in section 5. Discussion and conclusions are found in section 6.

2. A new method for EF identification

A powerful method for identifying the intrinsic EF sources in fusion devices standardly adapted in tokamaks is the compass scan. However, this is not a disruption-free technique being based on the triggering of a locked mode. The locked mode can indeed lead to a plasma disruption during the execution of the compass scan test, when the plasma current is in the flat-top phase, as shown in the MAST-U case presented in figure 2 on the left. Disruptions can occur also after the execution of the

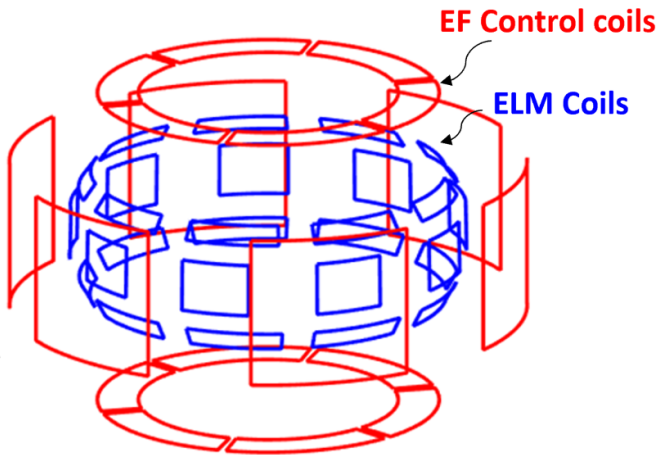


Figure 1. Geometry of error field actuators in ITER: the EF control coils (in red) and the ELM coils (in blue).

compass scan, when the plasma current is ramping down, as in the JET case reported in figure 2 on the right. Here, a residual locked mode was present despite the EF correction current has been switched off and its amplitude increased during the plasma termination.

Such dynamics cannot be tolerated in future disruption-averse tokamaks such as ITER and SPARC. To overcome this issue, the non-disruptive compass scan method has been designed and tested in the DIII-D tokamak in the $I_P = 0.8$ MA, $B_T = 1.4$ T Ohmic plasma scenario [17]. Similar to the conventional compass scan, an increasing probing field is applied until a magnetic island forms, but once this event is detected in real-time by the locked mode detector, as shown in figure 3 on the left, the plasma control system engages asynchronous control waveforms that enable prompt healing of the magnetic island. Magnetic island healing is achieved with a double action: (1) the current in the EF correction coils is reduced as quickly as possible, to remove the island drive, and (2) the density is increased, to stabilize the magnetic island.

To assess the portability of the non-disruptive compass scan method to ITER, dedicated experiments have been performed at JET and in MAST-U Ohmic plasma scenarios, with $I_P = 1.8$ MA, $B_T = 2.1$ T and $I_P = 0.75$ MA, $B_T = 0.5$ T, respectively. In both these devices, 4 EF correction coils, located external to the vacuum vessel, have been exploited to induce probing $n = 1$ magnetic fields. Promising results have been obtained, which demonstrated the high fidelity of the method and allowed us to gather a series of lessons learned that are of fundamental importance towards ITER and SPARC.

In particular, at JET, the magnetic island healing has been achieved not only by gas puff, as in DIII-D, but also with pellet injection, as reported in figure 4. The locked mode is stabilized when the plasma density increases at least 15% which can be reached by pellet injection in a faster time scale with respect to gas puff, as shown in panel (b). This result paves the way for using pellets to increase the density in ITER, which is the preferable actuator because of the slow time response of the gas valves and better particle penetration of pellets.

For the execution of these non-disruptive compass scan experiments, a real-time locked mode detector has been designed and included in the JET real time control system to initiate the asynchronous EFCC/density control. On the other hand, for the offline analyses, the dynamics of the locked mode has also been investigated, besides the commonly used observers (i.e. density drop, temperature flattening), through a novel approach which consists in looking for signatures of Beta Alfvén Eigenmodes, as proposed in [22, 23]. The locked mode formation is indeed accompanied by the appearance of MHD activities in the Mirnov spectrogram, which correspond to two lines with initially slightly different frequencies, i.e. 9 kHz and 12 kHz, as reported in figures 4(d) and (e). The lower MHD branch, with initial 9 kHz frequency, has a time evolving frequency. Its frequency depends on the locked mode amplitude, so on the island width. On the other hand, the higher MHD branch, with initial 12 kHz frequency, has a nearly constant frequency and could be associated with the presence of the $m = 3$, $n = 1$ magnetic island being the external 3D field applied made up of a spectrum of poloidal harmonics, as described in [24].

It is worth reporting that if the density cannot be raised sufficiently, the magnetic island is not healed. This has been the cause of plasma disruptions in non-disruptive compass scan tests performed at JET. An example is reported in figure 5. In the discharge plotted in black, as the locked mode onset has been detected by the JET real-time control system, an increase of plasma density has been requested by injecting for 0.8 s 2 mm Deuterium pellets paced at 7 Hz. As reported in panel (b), the plasma density slightly varies and its increase is not sufficient to stabilize the locked mode which eventually grows in amplitude, finally leading to a plasma disruption. On the other hand, in the discharge highlighted in blue, pellets injected at 14 Hz for 2 s have been requested, which efficiently increase the density. Based on the tests performed at JET, the pellet injection settings used in this later discharge are the optimal ones to effectively stabilize the magnetic island.

Another lesson learnt during testing the non-disruptive compass scan method in MAST-U is the importance of the locked mode detector, which initializes the asynchronous EFCC/density control. Unfortunately, such a real-time algorithm was not available in MAST-U control system and the triggering action has been set up empirically based on the knowledge of the locked mode onset in the conventional compass scan.

The discharge reported in black in figure 6 shows as an example a conventional compass scan test in MAST-U, where a locked mode has been triggered at $t = 0.37$ s because of the application of the probing field. The signature of locked mode onset, besides the magnetics, can be clearly seen on the time behaviour of the plasma density, which presents a sharp decrease as reported in panel (c). When testing the non-disruptive compass scan in the discharge plotted in blue, the empirical mode onset time has been used to switch off the EF correction current and to request a density increase, which allows the magnetic island healing. However, if the triggering

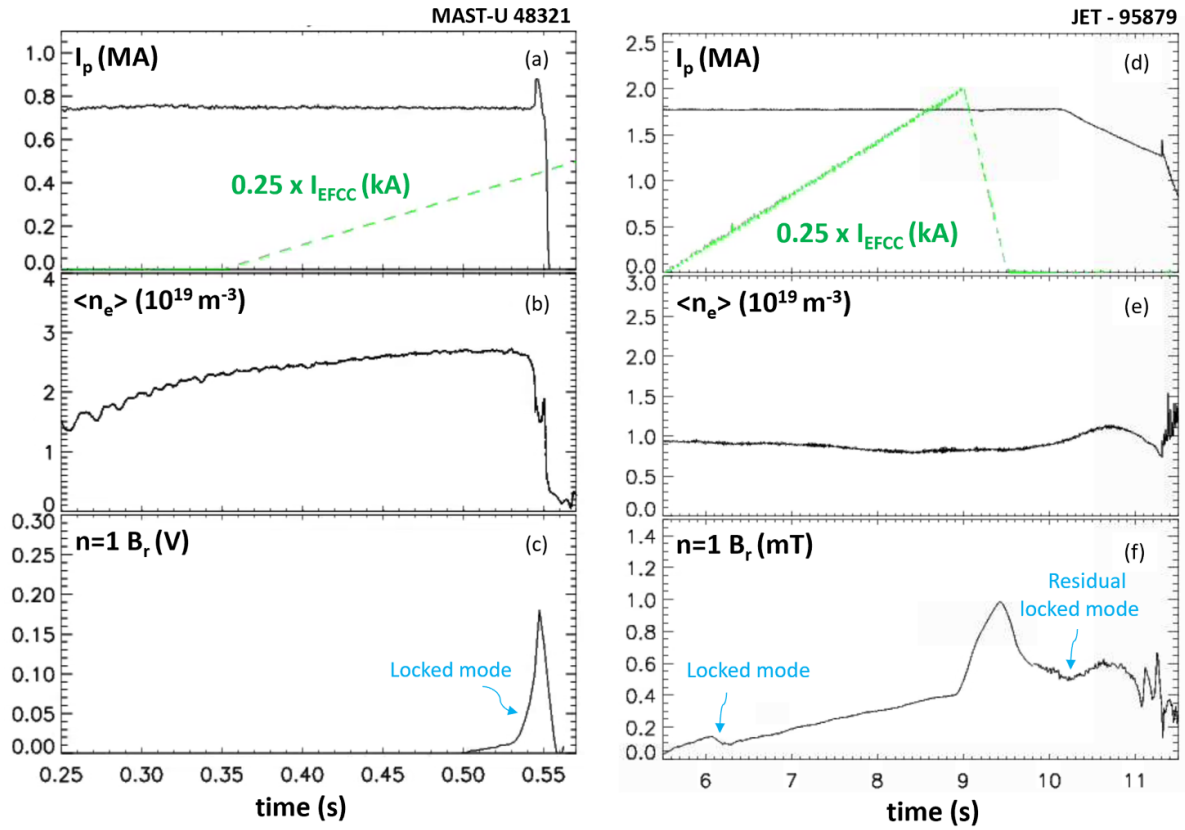


Figure 2. Time behaviour of (a)–(d) plasma current, (b)–(e) plasma density, (c)–(f) compensated $n = 1$ radial magnetic field during the execution of compass scan tests in a $I_p = 0.75$ MA, $B_T = 0.5$ T Ohmic plasma scenario in MAST-U (on the left) and in a $I_p = 1.8$ MA, $B_T = 2.1$ T Ohmic plasma scenario at JET (on the right).

time is set up earlier on, at $t = 0.35$ s, as in the discharge plotted in red, the locked mode is not triggered, rendering the experiment useless.

It is important to stress that the non-disruptive compass scan relies on an accurate detection of the magnetic island onset. The detection of magnetic island, standardly based on magnetic field measurements, is expected to be one of the main metric in the disruption prediction algorithm, and as such would be available in early device operations. However, during the non-disruptive compass scan tests, a procedure that allows magnetic measurements to be compensated from the external magnetic fields induced by the EF actuators, needs to be applied to guarantee a robust and high fidelity mode detection. For this purpose, studies have been carried out at JET to define new locked mode detectors for initiating the magnetic island healing as reported in [22]. Thanks to their simplicity and robustness, such locked mode detectors can be straightforwardly applied in the ITER plasma control system and be exploited during EF detection pulses scheduled in the first ITER plasma operations.

The non-disruptive compass scan method necessitates the enhancement of functionalities in the real-time control system compared to the conventional compass scan for accurately detecting the locked mode and initiating asynchronous EF current/density control. Nevertheless, it offers several advantages. Firstly, it prevents plasma disruption, and secondly, it reduces the required number of pulses for EF

identification. The limitation on the number of compass scan tests during the plasma current flat-top phase is primarily dictated by the available solenoid flux, contrasting with disruption events.

3. Modelling of magnetic island healing

In this section, the magnetic island mechanism has been modelled to improve our understanding on the required density increase and to explain the experimentally observed behaviour. For these purposes, the RFXlocking cylindrical code [25] has been used. It has been adapted to JET geometry by taking an effective cylindrical minor radius $a = a_{JET} \sqrt{\kappa}$, with $a_{JET} = 1$ m, $\kappa = 1.6$, and by considering the magnetic boundary made up of two thin shells: the vacuum vessel located at $r_\nu = 1.3a$, with time constant $\tau_\nu = 3$ ms, and the support structure at $r_b = 1.7a$, with $\tau_b = 30$ ms, as in [26]. The EFCC set, placed at $r_c = 1.8a$, is also included.

Given the low- β Ohmic regime under consideration, the equilibrium is set using a zero-pressure and a generalized Wesson-like current profile $\mu_0 \mathbf{J}_0(r) = \sigma(r) \mathbf{B}_0(r)$, with $\sigma(r) = 2((1 - (r/a)^{\alpha_1})^{\alpha_2} / R_0) q(0)$, μ_0 the magnetic permeability, \mathbf{J}_0 the equilibrium current density, R_0 the major radius, $q(0)$ the on-axis safety factor [27]. By taking $\alpha_1 = 2.8$, $\alpha_2 = 5$ we get a tearing-stable equilibrium, suitable to simulate the locked mode formation by EFCC.

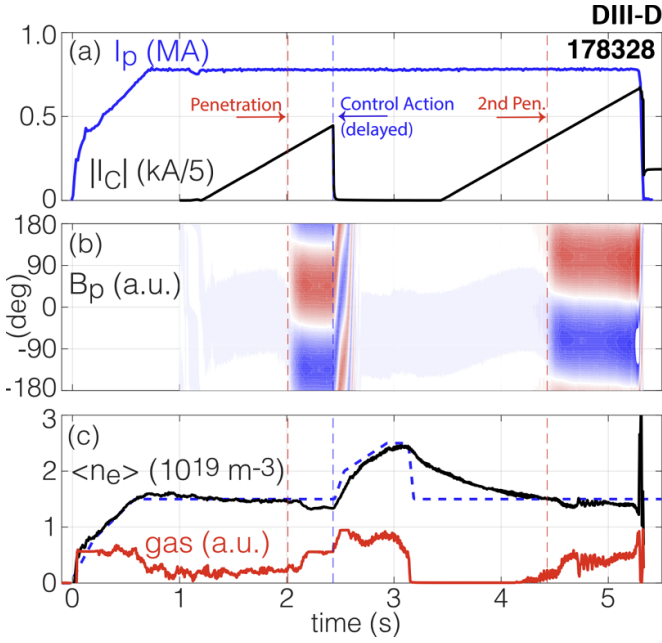


Figure 3. Time behaviour of (a) plasma current, (b) outboard midplane poloidal/radial magnetic field and (c) density of DIII-D non-disruptive compass scan test performed in DIII-D.

The radial profile of the complex radial field harmonic $\psi^{m,n}(r, t) \equiv -i r b^{m,n}_r(r, t)$ related to the $m = 2, n = 1$ magnetic island is computed by solving Newcomb's equation where $b^{m,n}_r$ is the radial magnetic field of the m, n mode, including the effects of the external passive and active conductive structures. In particular, the radial magnetic field diffusion across the two shells is described by the thin-shell dispersion relation [28].

Regarding the physics at the $q = 2$ surface (located at $0.86a$) two distinct regimes are assumed: (i) the linear viscous-resistive-regime [29], to simulate the penetration at the $q = 2$ surface of the EFCC magnetic perturbation, starting from a tearing-mode-free plasma. The resistive diffusion time τ_R is computed by Spitzer resistivity with a neoclassical correction ($\tau_R \approx 1$ s), (ii) the Rutherford non-linear regime, to simulate the subsequent evolution of the width of the locked magnetic island thus formed. In the Rutherford regime, the island phase is evolved by assuming the island to be frozen within the electron fluid at the $q = 2$ surface (no-slip constraint). In turn, the electron velocity is obtained by adding the diamagnetic drift to the ion (single-fluid) velocity.

In particular, the ion velocity is the solution of single-fluid toroidal and poloidal motion equations, similar to those considered in [28]. They include: (i) the electromagnetic torque (EM) developed by the interaction between the magnetic island and the external conductive structures; (ii) the viscous torque produced by the kinematic perpendicular viscosity ν and the fluid motion; (iii) a phenomenological poloidal flow damping term; (iv) a phenomenological momentum source. The perpendicular viscosity is quantified through the viscous diffusion time $\tau_\nu = a^2/\nu$, taken of the same order of the estimated energy confinement time τ_E ($\tau_E \approx 0.2$ s).

The basic simulation is displayed in figure 7. In the viscous-resistive regime, as the current in the EFCC is ramped up (black trace figure 7(a)), a magnetic island begins to form, due to the finite resistivity which allows the change of the topology of the magnetic surfaces. However, in the terminology of [29], it is a 'suppressed island', not subjected to the no-slip constraint. At about 1 s a sharp increase of the island width is observed: this marks the mode-penetration, which means that the island enters the non-linear regime subjected to the no-slip constraint and locked to the external magnetic field perturbation.

The EFCC current is then kept at a finite value to mimic the presence of an intrinsic residual EF. In the non-linear regime the island width saturates at $W/a \approx 0.06$ (figure 8(a) blue trace), though the underlying equilibrium is tearing stable. The island phase φ_w , reported in black in figure 8(b), promptly reaches a stationary value, but a finite shift $\Delta\varphi$ with respect to the EF phase φ_{EFCC} is observed (red trace, same figure).

This shift is required by the balance, in stationary conditions, between the EM torque produced by interaction of the island with the EF, and the viscous torque due to the fluid motion, which acts to drag the island. Schematically, the torque balance for a locked island can be written as

$$\text{const} \times |I_{\text{EFCC}}^{2,1}| W^2 \sin(\Delta\varphi) = -\rho\nu\omega_0, \quad (1)$$

where ρ is the mass density, and ω_0 the angular frequency of an island rotating with the unperturbed fluid (i.e. under zero EM torque) at the $q = 2$ surface. In this expression, $I_{\text{EFCC}}^{2,1}$ is the value which simulates the presence of the residual EF. In equation (1) the left-hand side describes the EM torque, whereas the right-hand side represents the viscous torque. The constant in the left term incorporates various equilibrium dependent quantities.

For fixed values of $I_{\text{EFCC}}^{2,1}$ and W equation (1) shows that $|\Delta\varphi|$ tends towards $\pi/2$ as the magnitude of the viscous torque (the right-hand side) increases. At $|\Delta\varphi| = \pi/2$ a further increase of the viscous torque prevents the possibility of satisfying the torque-balance condition, hence the island unlocks and begins to rotate. Therefore, increasing the plasma density, i.e. ρ , is a recipe to spin-up a locked island and stabilizing it, if ν and ω_0 do not decrease.

This method has been experimentally tested and interpreted by simulations in [17]. Here, we try to go deeper in the mechanism responsible of the island spin-up and subsequent stabilization. A set of simulations are then performed by increasing the density, after the locked island has formed, while keeping ν and ω_0 unaltered. The effect of increasing ρ by 5%, 10% and 25%, from $t = 2$ s onwards, is reported in figure 8. A 5% increase is not enough to unlock the island. But, above a 10% density increase the island spins-up after reaching the critical value $|\Delta\varphi| = \pi/2$ (figure 8(b)). At the same time, the width decreases up to the complete disappearance of the island (figure 8(a)), due to the fact that rotation suppresses the EF destabilizing effect.

The assumption of keeping ν and ω_0 constant while increasing the mass density is justified by experimental analyses. Indeed, a dependence of the rotation profile on density is only

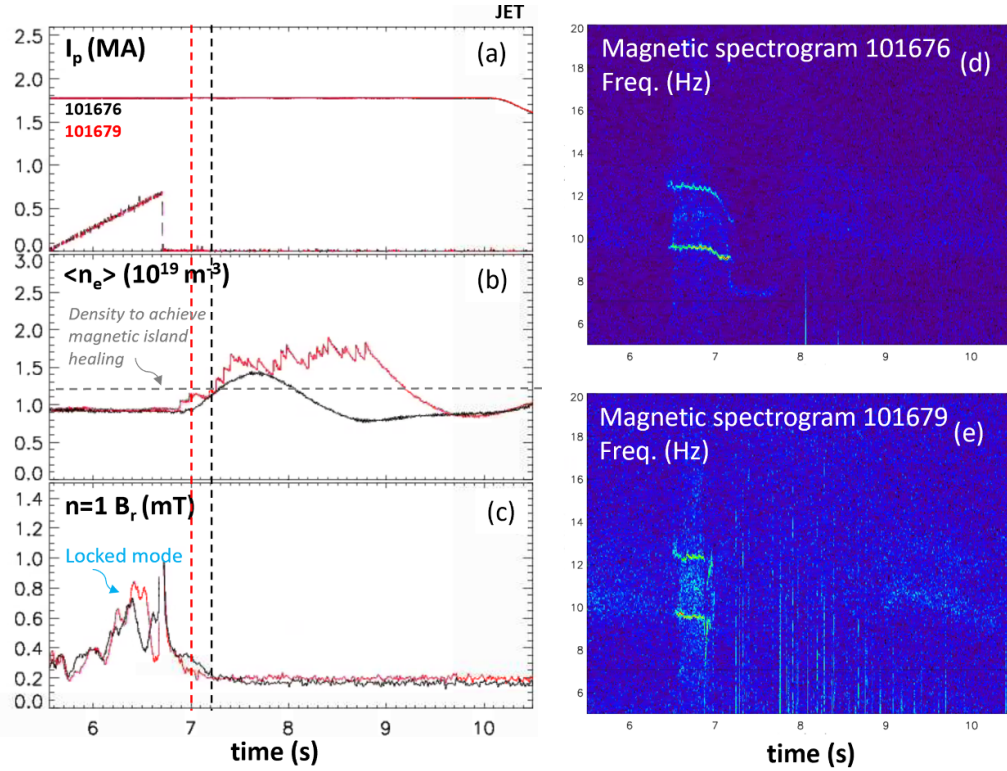


Figure 4. Time behaviour of (a) plasma current, (b) plasma density, (c) compensated $n = 1$ radial magnetic field during and (d)–(e) magnetic spectrograms of non-disruptive compass scan tests in the $I_p = 1.8$ MA, $B_T = 2.1$ T Ohmic plasma scenario at JET where magnetic island healing has been achieved by gas puff (in black) and by pellet injection (in red).

observed in the core region, during the non-disruptive compass scan experiment, while at the $q = 2$ surface the profile remains unaltered. Moreover, the energy confinement time does not vary while changing the plasma density. This suggests that the plasma is in the saturated Ohmic regime [30], thus the kinematic viscosity $\nu \approx a^2/\tau_E$ can be kept constant with density.

These modelling insights are in good agreement with the JET experimental results reported in figure 4 and similar studies performed with the TM1 code, described in [17]. They also suggest that a faster density increase, as the one obtained by pellet injection, guarantees a quicker magnetic island healing.

4. Development of controllers for EF identification in ITER

In preparation to the execution of the non-disruptive compass scan method in the first plasma ITER operations, a series of real-time algorithms are being finalized, i.e. the locked mode detector and the asynchronous control of current in the EF actuators and plasma density.

The locked mode detector aims at identifying non-rotating, non-axisymmetric magnetic field perturbations associated with the onset of a locked mode and relies on a wide coverage of magnetic field sensors available in ITER [31], such as the 9 MHD saddle coils, which measure the normal magnetic field component and are evenly spaced and located in each sector of the machine, external to the vacuum vessel, and

the 18 high-field tangential pickup coils, which measure the local tangential magnetic field component and are deployed on the inner surface of the vacuum vessel.

During EF identification studies, the magnetic field measurements used in input to the real-time detector shall be compensated by the external magnetic field induced by the EF actuators in order to guarantee a reliable and robust detection of the locked mode formation. As documented in [22], an ad-hoc locked mode detector algorithm, based on compensated magnetic field measurements, has been designed and successfully tested at JET and paves the way for its exploitation in ITER and beyond.

When executing the non-disruptive compass scan experiments, the locked mode detector has the primary role of enabling the control actions for magnetic island healing which is achieved by the asynchronous EF current and density controller. Such a controller, as the locked mode formation is detected, requests a prompt reduction of current in the EF actuator and simultaneously a density rise allowing the magnetic island stabilization.

In preparation to ITER experiments, the proportional-integral (PI) current regulator designed for the Engineering Operation of the EFCC system [32], the primary system for EF control, has been tuned to meet specific requirements. Indeed, effective EFCCs is achieved by effectively tracking the current ramp-up waveforms in the EFCC until the locked mode is detected. Then the current in the coils shall be discharged as fast as possible, by also minimizing the current undershoots.

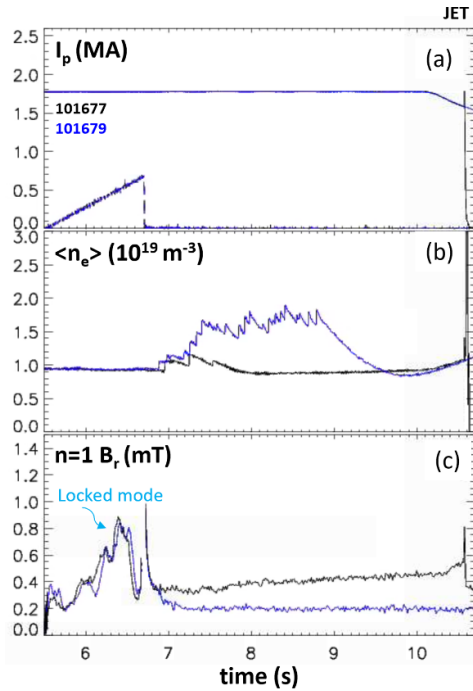


Figure 5. Time behaviour of (a) plasma current, (b) plasma density, (c) compensated $n = 1$ radial magnetic field during the execution of the non-disruptive compass scan tests in the $I_p = 1.8$ MA, $B_T = 2.1$ T Ohmic plasma scenario at JET where 7 Hz for 0.8 s (in black) and 14 Hz for 2 s (in blue) pellets have been injected to heal the magnetic island.

This performance is the result of fine-tuning the PI gains, with the optimal set having a proportional gain of 1 and an integral gain of 0.15, as depicted by behaviour of modelled EFCC current shown in black in figure 9(a). It is noteworthy that utilizing a non-optimal gain set, as indicated by the red curve in the same figure, introduces undesirable EFCC current oscillations.

As the current in the EFCCs is discharged, the asynchronous controller allows an increase of density, which will be achieved in ITER by pellet injection because of the faster density response.

The level of density increase needed to heal the magnetic island is not known at present, given the EF sources still need to be determined. However, an assessment of the density raise associated with pellet injection has been carried out by ASTRA code [33], complemented with SMART modelling [34] to simulate the high field side pellet injection from the equatorial location.

Such a study has been carried out considering the low density Ohmic current flat-top phase of $I_p = 5$ MA, $B_t = 2.65$ T ITER scenario for various basic sizes of pellets assumed for ITER. The simulated behaviour of plasma density in presence of a single and multiple pellet injection at different sizes is reported, as an example, in figures 9(b) and (c). Note that the relative increase of plasma density depends on the pellet size. Indeed, it is possible to increase plasma density by 40% by injecting one medium-size pellet (90 mm^3) or by injecting

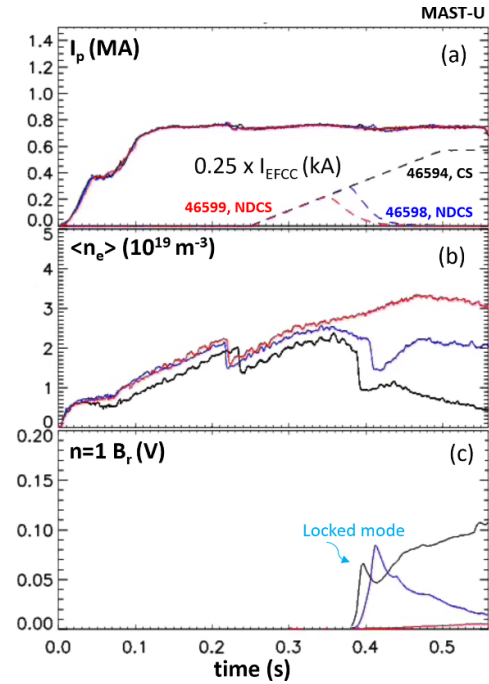


Figure 6. Time behaviour of (a) plasma current, (b) plasma density, (c) compensated $n = 1$ radial magnetic field during the execution of the non-disruptive compass scan tests in the $I_p = 0.75$ MA, $B_T = 0.5$ T Ohmic plasma scenario in MAST-U.

multiple smaller pellets. Note the study of multiple large pellet injection (90 mm^3) has not been reported because after the second pellet arrival, the density will exceed the Greenwald limit. The injection of multiple pellets is the preferable option to increase the pellet injector reliability.

5. EF control in low density, low torque ITER relevant regimes

Experiments on model-based EF control [10, 13, 20] rely on an accurate understanding of the spectral composition of the intrinsic EF, from which an assessment of the best strategy for correction can be designed based on how 3D fields couple to the plasma. To contribute on the identification of the optimal EF correction approach towards ITER operation, EF control studies have been carried out in ASDEX-Upgrade in challenging ITER relevant regimes: the low torque, low density Ohmic plasma scenario.

ASDEX-Upgrade is the suitable test-bed experiment for conducting this type of study. On one hand, it is characterized by the presence of an the intrinsic EF source, due to the feedthroughs of the poloidal field coils, which are located on the upper and lower part of the tokamak and toroidally localized at around $\phi = 320$ deg [35]. On the other hand, ASDEX-Upgrade is equipped with an EF correction coil, known as the B-coil set, consisting of 8 coils located above (BU) and 8 coils below (BL) the device midplane. These coils are internal to the vacuum vessel and powered by independent power supplies [36].

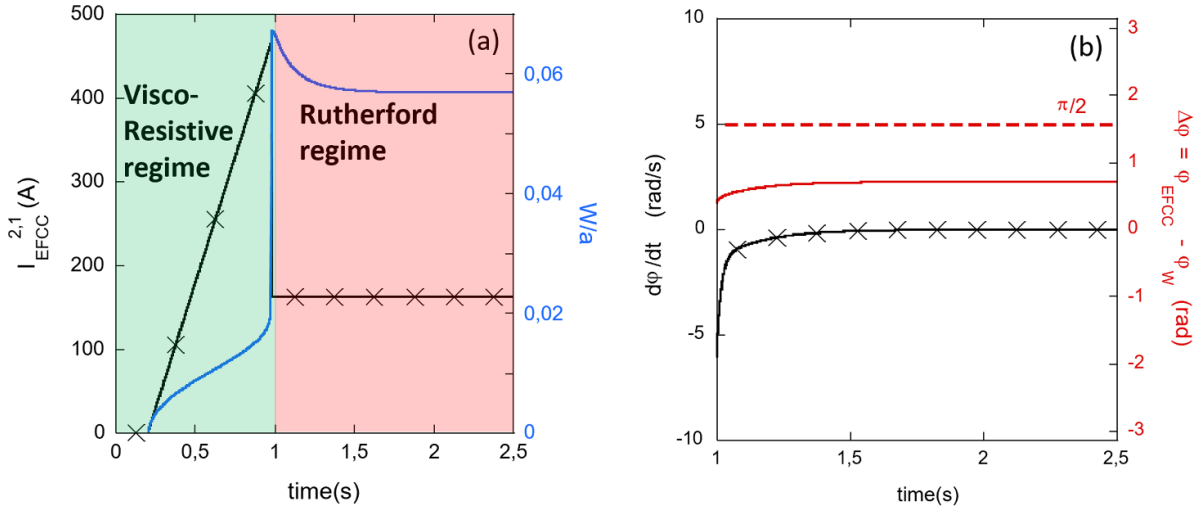


Figure 7. (a) Time evolution of EFCC current (in black) and normalized island width (in blue). The evolution is dictated by the visco-resistive regime in the time interval highlighted in green, while by the Rutherford regime after mode penetration, which occurs at about 1 s. In this regime the EFCC current is kept at a finite value to mimic the presence of an intrinsic residual EF. (b) Island phase velocity (in black) and $\Delta\varphi$, the difference between the island and EF phases, (in red), in the Rutherford regime.

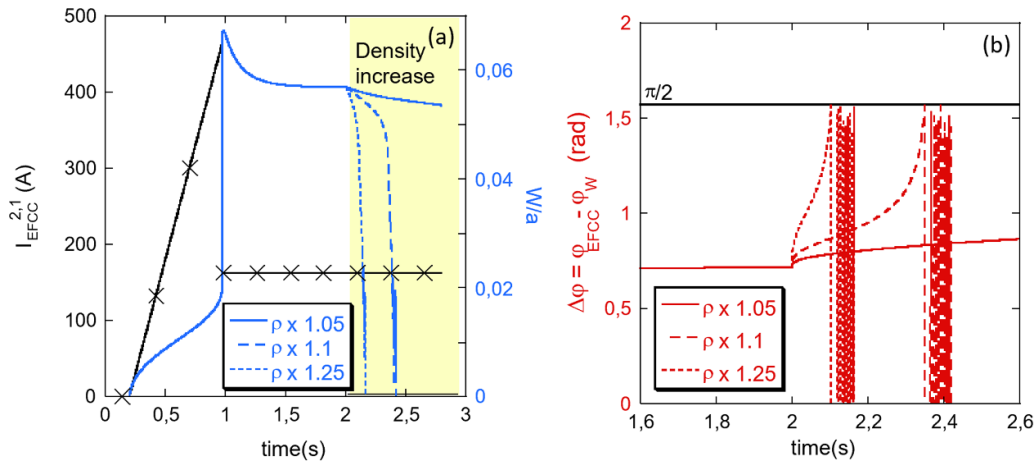


Figure 8. (a) Time evolution of EFCC current (in black) and normalized island width (in blue) and (b) $\Delta\varphi$, the difference between the island and EF phases (in red) for different values of mass density.

To identify EF correction recipes, two codes have been applied and tested: the CAFE code, which is a purely electro-magnetic field model, which includes the poloidal field coils systems and the presence of their feedthroughs [37, 38], and the MARS-F code, which is able to calculate the response of the plasmas to the known intrinsic EF source [39]. Plasma response effects including poloidal mode coupling and field amplification are indeed key elements in quantitatively determining the penetration threshold and optimal correction of EFs [10, 13].

The criterion adopted for EF correction was based on the full cancellation of the normal magnetic field amplitude aligned with the pitch of the field lines at the $q = 2$ surface, both in vacuum approximation, so deduced by CAFE modelling, and including the plasma response, obtained by coupling CAFE with the MARS-F code.

These model-based EF correction recipes have been tested in $I_P = 0.8$ MA, $B_T = 1.5$ T plasmas in the low density

regime, and explored by ramping down the density, to mimic the first ITER operation at low-plasma rotation. The metric that has been used to judge the efficiency of the EF correction recipe is the achievement of a lower density level with respect to the reference discharge, while avoiding the plasma disruption.

Figure 10 represents three similar plasma discharges where no EF correction has been applied (in red) and where vacuum (in green) and plasma response (in cyan) EF correction currents have been tested in feedforward from $t = 1$ s. Consistently with previous findings [10, 19, 40], the EF correction strategy that does not neglect the response of plasma to the applied EF performs better, allowing to access the operation at lower densities than otherwise in ASDEX-Upgrade. This method of correction, however, requires the full knowledge of the EF source. It is crucial for the early ITER operation to prioritize the validation of the EF model. This can be achieved through laser tracking, digital photogrammetry methods, and

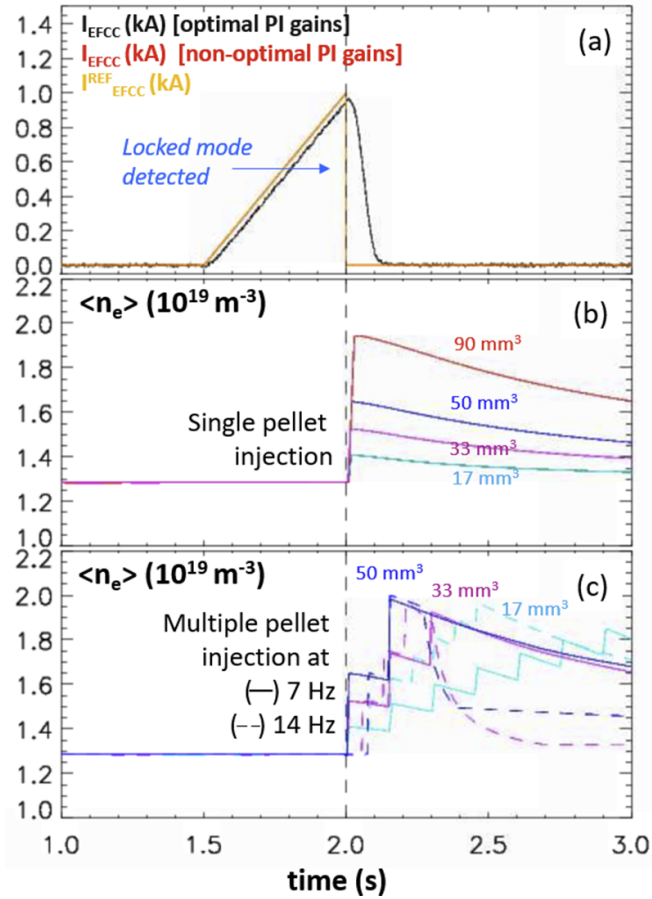


Figure 9. Time evolution of (a) prescribed trajectory (in orange) and simulated $n = 1$ EFCC current when using the optimal PI gain set (in black) and non-optimal one (in red) and (b)–(c) plasma density from ASTRA modelling predictions in presence of single and multiple pellet injections at various sizes of pellet in the $I_p = 5$ MA, $B_t = 2.65$ T divertor ITER scenario.

EF identification studies outlined in section 2, to ensure a confident application of EF correction.

Once the source geometry of the intrinsic EF is fully known, it needs to be implemented in a 3D electro-magnetic code, and complimented with plasma response modelling, making it more challenging to provide real-time correction by this method. For this reason, in present fusion devices EF correction currents are pre-calculated before experiments and applied in a feedforward manner. However, upcoming tests aim to advance this approach by integrating it into a real-time feedback scheme.

It is worth reporting that the same of EF correction approach has been also adopted recently in the high-beta regime, as documented in [21], improving the achievable β_N by 10%.

6. Conclusions

In this work, robust and reliable methodologies that should be adopted for identifying and correcting EF sources in ITER have been presented, considering cross-machine studies carried out in ASDEX-Upgrade, DIII-D, JET and MAST-U.

This set of experiments (i) shows that the non-disruptive compass scan method is a valuable alternative to the conventional compass scan, permitting the minimization of disruption risk, by achieving the magnetic island healing, and the optimization of the experimental time, allowing more than one EF identification test in just a single discharge as the solenoid flux allows, (ii) provides a series of lessons learn/insights that would be of primary importance for ITER commissioning, such as the careful optimization of pellet injection settings to guarantee an effective magnetic island stabilization, (iii) motivated the development of controllers, such as new detectors for locked mode and the asynchronous EF current/density controller by pellets, and the establishment of workflow strategies for calculating model-based correction strategies that, thanks to their portability, can be transferred to ITER and to next step fusion devices.

In preparation to EF identification and control experiments related in ITER, it is essential to allocate dedicated efforts in the coming years to acquire knowledge of intrinsic EF sources using laser tracking and photogrammetry techniques. Additionally, there is a need for the development and testing of EF control metrics aimed at reducing rotation braking. In ITER, unlike contemporary medium-sized devices

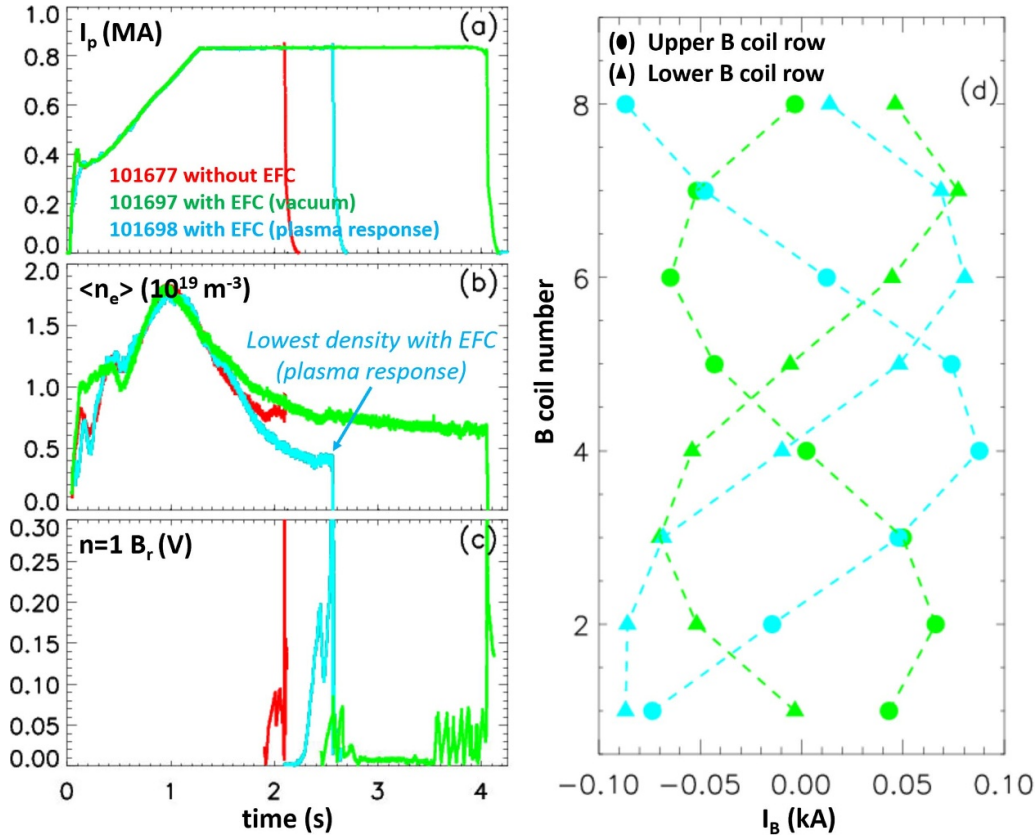


Figure 10. Time behaviour of (a) plasma current, (b) density, (c) $n = 1$ Br amplitude in three similar $I_p = 0.8$ MA, $B_t = 1.5$ T Ohmic discharges performed in ASDEX-Upgrade where the low density regime prone to a locked mode has been explored (red, reference) and model-based vacuum (in green) and plasma response (in cyan) EF correction strategies have been tested. (d) Distribution of B coil correction currents as foreseen by vacuum modelling (in green) and including plasma response (in cyan). The symbols have been used to distinguish the current level in the upper and in the lower B coil rows.

where rotation is primarily induced by neutral beam injection, the plasma inertia will be significantly larger. However, the torque increase, at best, is only marginal. This results in a low rotation regime, offering less effective shielding of EFs. Consequently, the plasma scenario becomes more susceptible to locked modes and plasma disruptions.

In this context, the design of the ITER plasma control system assumes significant importance. This is because the EFCC and the ELM coil systems in ITER serve several purposes. They are not only employed for EF minimization but also play crucial role in ELM and neoclassical tearing mode control. The latter involves locking the magnetic island by applying a proxy EF in front of the electron cyclotron launcher, as recently proposed in [41]. Consequently, the development of a set of real-time flexible functionalities becomes imperative to effectively orchestrate the same actuators for multiple purposes based on the plasma state.

Acknowledgments

This work has been carried out within the framework of the EUROfusion Consortium, funded by the European Union via the Euratom Research and Training Programme (Grant Agreement No. 101052200 EUROfusion). Views and opinions

expressed are however those of the author(s) only and do not necessarily reflect those of the European Union or the European Commission. Neither the European Union nor the European Commission can be held responsible for them. The views and opinions expressed herein do not necessarily reflect those of the ITER Organization. This material is based upon work supported by the US Department of Energy, Office of Science, Office of Fusion Energy Sciences, using the DIII-D National Fusion Facility, a DOE Office of Science user facility, under Award(s) DE-FC02-04ER54698 and DE-SC0022270. Disclaimer: This report was prepared as an account of work sponsored by an agency of the United States Government. Neither the United States Government nor any agency thereof, nor any of their employees, makes any warranty, express or implied, or assumes any legal liability or responsibility for the accuracy, completeness, or usefulness of any information, apparatus, product, or process disclosed, or represents that its use would not infringe privately owned rights. Reference herein to any specific commercial product, process, or service by trade name, trademark, manufacturer, or otherwise does not necessarily constitute or imply its endorsement, recommendation, or favouring by the United States Government or any agency thereof. The views and opinions of authors expressed herein do not necessarily state or reflect those of the United States Government or any agency thereof.

ORCID iDs

L. Piron  <https://orcid.org/0000-0002-7928-4661>
 C. Paz-Soldan  <https://orcid.org/0000-0001-5069-4934>
 L. Pigatto  <https://orcid.org/0000-0002-0556-0440>
 P. Zanca  <https://orcid.org/0000-0003-3208-976X>
 O. Sauter  <https://orcid.org/0000-0002-0099-6675>
 T. Putterich  <https://orcid.org/0000-0002-8487-4973>
 P. Bettini  <https://orcid.org/0000-0001-7084-4071>
 M. Bonotto  <https://orcid.org/0000-0001-9147-7506>
 G. De Tommasi  <https://orcid.org/0000-0002-8509-7176>
 P. De Vries  <https://orcid.org/0000-0001-7304-5486>
 Q. Hu  <https://orcid.org/0000-0002-8877-4988>
 N.C. Logan  <https://orcid.org/0000-0002-3268-7359>
 M. Lennholm  <https://orcid.org/0000-0002-3444-3999>
 M. Mattei  <https://orcid.org/0000-0001-7951-6584>
 T. Ravensbergen  <https://orcid.org/0000-0001-7347-5515>
 D. Ryan  <https://orcid.org/0000-0002-7735-3598>
 B. Sieglin  <https://orcid.org/0000-0002-9480-4434>
 W. Suttrop  <https://orcid.org/0000-0003-0983-8881>
 D. Terranova  <https://orcid.org/0000-0001-9339-283X>

References

- [1] Strait E.J. et al 2011 *Phys. Plasmas* **22** 021803
- [2] Callen J.D. et al 2015 *Nucl. Fusion* **51** 094026
- [3] Scoville J.T., La Haye R.J., Kellman A.G., Osborne T.H., Stambaugh R.D., Strait E.J. and Taylor T.S. 1991 *Nucl. Fusion* **31** 875
- [4] Menard J.E. et al 2010 *Nucl. Fusion* **50** 045008
- [5] Wolfe S.M. et al 2005 *Phys. Plasmas* **12** 1
- [6] Maraschek M. et al 2013 Measurement and impact of the n=1 intrinsic error field at ASDEX Upgrade 40th EPS Conf. on Plasma Physics, EPS 2013 (Espoo, Finland, 1–5 July 2013) p 4.127 (available at: <http://ocs.ciemat.es/EPS2013PAP/pdf/P4.127.pdf>)
- [7] Buttery R.J. et al 1999 *Nucl. Fusion* **39** 1827–35
- [8] Buttery R.J., Benedetti M.D., Hender T.C. and Tubbing B.J.D. 2000 *Nucl. Fusion* **40** 807–19
- [9] Kirk A., Liu Y., Martin R., Cunningham G. and Howell D. 2014 *Plasma Phys. Control. Fusion* **56** 104003
- [10] Liu Y.Q., Kirk A. and Thornton A.J. 2014 *Plasma Phys. Control. Fusion* **56** 104002
- [11] Wang H.-H. et al 2016 *Nucl. Fusion* **56** 066011
- [12] Schaffer M. et al 2011 *Nucl. Fusion* **51** 103028
- [13] Paz-Soldan C., Buttery R.J., Garofalo A.M., Hanson J.M., La Haye R.J., Lanctot M.J., Park J.K., Solomon W.M. and Strait E.J. 2014 *Nucl. Fusion* **54** 073013
- [14] In Y., Park J.K., Jeon J.M., Kim J. and Okabayashi M. 2015 *Nucl. Fusion* **55** 043004
- [15] Puiatti M.E. et al 2015 *Nucl. Fusion* **55** 104012
- [16] ITER document management system: DMS heat load mitigation targets 57 VT5Y (private communication)
- [17] Paz-Soldan C., Hu Q., Logan N.C. and Park J.-K. 2022 *Nucl. Fusion* **62** 126007
- [18] Park J.-K., Boozer A.H., Menard J.E., Garofalo A.M., Schaffer M.J., Hawryluk R.J., Kaye S.M., Gerhardt S.P. and Sabbagh S.A. 2009 *Phys. Plasmas* **16** 056115
- [19] Park J.-K., Boozer A.H., Menard J.E. and Schaffer M.J. 2008 *Nucl. Fusion* **48** 045006
- [20] Paz-Soldan C., Lanctot M.J., Logan N.C., Shiraki D., Buttery R.J., Hanson J.M., La Haye R.J., Park J.-K., Solomon W.M. and Strait E.J. 2014 *Phys. Plasmas* **21** 072503
- [21] Igochine V., Bonotto M., Gude A., Maraschek M., Pigatto L., Bettini P., Liu Y.Q., Piron L., Voltolina D. and Zohm H. 2023 *Plasma Phys. Control. Fusion* **65** 062001
- [22] Piron L. et al 2023 *Fusion Sci. Eng.* **195** 113957
- [23] Pucella G. et al 2022 *Plasma Phys. Control. Fusion* **64** 045023
- [24] Chapman I.T., Hender T.C., Howell D.F., Erements S.K., Gryaznevich M.P., Shibaev S., Stamp M.F., de la Luna E., Savchikov A. and Scannell R. 2007 *Nucl. Fusion* **47** L36–L40
- [25] Zanca P., Paccagnella R., Finotti C., Fassina A., Manduchi G., Cavazzana R., Franz P., Piron C. and Piron L. 2015 *Nucl. Fusion* **55** 043020
- [26] Piron L. et al 2023 *Fusion Sci. Eng.* **197** 114069
- [27] Wesson J.A. 2004 *Tokamaks* 3rd edn (Clarendon)
- [28] Gimblett C.G. 1986 *Nucl. Fusion* **26** 617
- [29] Fitzpatrick R. 1993 *Nucl. Fusion* **33** 1049
- [30] Parker R., Greenwald M., Luckhardt S.C., Marmor E.S., Porkolab M. and Wolfe S.M. 1985 *Nucl. Fusion* **25** 1127
- [31] ITER document management system: system_Design_Description_(DDD)_55.A0_Ma_3UYQGX_v6 (private communication)
- [32] De Tommasi G. et al 2022 *Fusion Eng. Des.* **185** 113317
- [33] Pereverzev G.V. and Yushmanov P.N. 2002 *ASTRA Automated System for TRansport Analysis* (Max-Planck-Institut Für Plasmaphysik) IPP-Report, IPP 5/98, February (available at: https://w3.pppl.gov/~hammett/work/2009/Astra_ocr.pdf)
- [34] Polevoi A.R. and Shimada M. 2001 *Plasma Phys. Control. Fusion* **43** 1525
- [35] Maraschek M. et al 2013 *Proc. 40th European Physical Society Conf. on Plasma Physics (Espoo)* P4.127
- [36] Suttrop W. et al 2009 *Fusion Eng. Des.* **84** 2
- [37] Voltolina D. et al 2019 Vacuum estimation of error field correction on ASDEX Upgrade 46th EPS Conf. on Plasma Physics (Milano, Italia) P4.1099
- [38] Bettini P. et al 2017 *IEEE Trans. Magn.* **53** 7204904
- [39] Liu Y.Q., Bondeson A., Fransson C.M., Lennartson B. and Breitholtz C. 2000 *Phys. Plasmas* **7** 3681
- [40] Park J.-K., Boozer A.H. and Glasser A.H. 2007 *Phys. Plasmas* **14** 052110
- [41] Nies R., Reiman A.H. and Fisch N.J. 2022 *Nucl. Fusion* **62** 086044